Available online at www.sciencedirect.com

ScienceDirect

IFAC PapersOnline CONFERENCE PAPER ARCHIVE

IFAC PapersOnLine 54-16 (2021) 320–326

Marine boundary layer tracking using an AUV with UKF based extremum seeking ⋆

Tim Benedikt von See * **Thomas Meurer** ** **Jens Greinert** *

* *GEOMAR Helmholtz-Center for Ocean Research Kiel (e-mail: {tsee, jgreinert}@geomar.de*

** *Chair of Automatic Control, Faculty of Engineering, Kiel University, (e-mail: tm@tf.uni-kiel.de)*

Abstract: Adaptive sampling and situational awareness for autonomous underwater vehicles (AUVs) is a major improvement in ocean research. By only sampling the feature of interest in a feature-relevant domain instead of a covering a whole area expensive ship time can be saved and at the same time a more comprehensive data set can be obtained. A classical marine example where adaptive sampling is useful is sampling of boundary layers such as the thermocline because the boundary layer thickness is very small compared to the depth of the water column. These boundary layers play an important role in many ocean related disciplines such as marine biology, physical oceanography and underwater acoustics. In this paper an unscented Kalman filter (UKF) based extremum seeking control (ESC) approach is presented to detect and track such boundary layers. Simulation results for different use cases are presented to show its effectiveness.

Keywords: AUV, Kalman filter, extremum seeking control, boundary layer tracking, thermocline

1. INTRODUCTION

Autonomous underwater vehicles (AUVs) have been used in a wide range of applications and the market for AUVs is expected to double or triple its volume within the next years according to MarketsandMarkets (2020). But even though AUVs have been used to autonomously find phenomena such as thermoclines, ocean fronts or hydrothermal vents, there is no commercial AUV with such build in capability. The main use of AUVs remains collecting data while following pre-defined geo-referenced paths. If only a specific feature is of interest this sampling method is suboptimal because the pre-defined path has to include every location where the feature is likely to occur. Such paths lead to data sets with only few samples of the feature of interest, thus having a poor data quality. Furthermore the mission time and therefore also expensive ship time is increased. Since the collected data is only post-processed on-ship or on-shore the adaption of the AUV mission is only possible for nearly static features but not for highly dynamic features such as internal waves.

The first adaptive sampling approaches with AUVs were used for detecting and tracking the thermocline which is the layer in the water column where the temperature gradient with respect to depth has its maximum. This layer typically coincides with the halocline and oxycline which are the layers with the maximum salinity and oxygen gradient, respectively. The detection of these layers is of interest because it determines if the entire water body is well mixed or if a barrier for sinking particles is created and it is a habitat for certain fauna. The aim of so far published adaptive sampling algorithms for thermocline detection and tracking was to shorten the classical Jo-Jo pattern that without adaptive sampling would range from the surface to the sea floor. In Petillo et al. (2010) the authors propose a method where the AUV first conducts a complete deep dive that is used to calculate the average temperature gradient with respect to depth. The water layer where the temperature gradient is larger than the average gradient is defined as the thermocline. A Jo-Jo pattern in this depth is planned and a regular complete dive is done to account for large scale variations in the thermocline. In Cruz and Matos (2010a), Cruz and Matos (2010b) a thermocline detection algorithm is presented that uses the vertical temperature gradient to detect the upper and lower part of the thermocline. The authors develop a state machine consisting of 4 states and a set of thresholds which are updated during the AUV mission based on the maximum gradient found on the last down or upward track. They present simulation results and data from a demonstration in a dam reservoir. In Zhang et al. (2010) a peak gradient method for thermocline tracking is presented. Here the water column is divided into depth bins and the largest gradient for neighboring bins is detected and defined as the mean thermocline depth. The next target depth is calculated as this depth plus or minus an extension depth to ensure complete sampling of the thermocline. The authors present simulation results followed by field data two years later in Zhang et al. (2012). All these algorithms rely on thresholds of the gradient of the water property. This might lead to incomplete sampling of the desired area in case of small-scale changes, e.g., zigzag evolution of the boundary layer, and in cases where more than one boundary layer is present. These conditions

⋆ The first author is funded through the Helmholtz School for Marine Data Science (MarDATA), Grant No. HIDSS-0005. Parts of the work of the first author have been performed at the Kiel University at the Chair of Automatic Control.

10.1016/j.ifacol.2021.10.111

occur, e.g., when there is an oxygen maximum layer within the water column. An approach that differs from these methods is presented in Antunes and Cruz (2019). Here an extremum seeking control (ESC) loop based on Krstić and Wang (2000) is used for the thermocline tracking with a vertical profiler. Simulation results for artificial and real thermocline data are presented and for the artificial data also a time dependence of the thermocline in considered. However the simulation data is very smooth so that a significant gradient is measurable at all times which for real world data is often not the case.

The approach proposed in this paper is also an extremum seeking control (ESC) method but an unscented Kalman filter (UKF) is used for the gradient estimation to improve the estimator performance. This was originally proposed in Lutz et al. (2019) for a gas engine. The improvement of the estimator performance by using an UKF is mainly due to the fact that the gradient is estimated iteratively. If the the covariances of the noise are exactly known the estimation error is reduced optimally in the least squares error sense. In contrast typically used ESC schemes as the one in Antunes and Cruz (2019) only use instantaneous data for the gradient estimation neglecting the cost function history. Furthermore an extension to a two stage approach is considered to deal with situations in which no gradient information is measurable to overcome the shortcomings of the approach of Antunes and Cruz (2019). The first ESC algorithms were developed in the 1950-1960s but did not gain much attention because of difficulties in their analytical treatment. Only around 2000 Krstić and Wang (2000) were able to provide a proof of stability for extremum seeking feedback control for general nonlinear dynamic systems. Since then ESC gained new attention and is an ongoing field of research, see Scheinker and Scheinker (2016), Radut (2017), Bhattacharjee and Subbarao (2021).

The paper is structured as follows. In Section 2 the proposed ESC method and its application to boundary layer tracking is described. The AUV model, simulation framework and simulation data are presented in Section 3 followed by simulation results for three use cases in Section 4. A conclusion and outlook is given in Section 5.

2. UNSCENTED KALMAN FILTER BASED EXTREMUM SEEKING CONTROL

The proposed ESC loop based on Lutz et al. (2019) is shown in Fig. 1. The input/output map at the top is composed of the nonlinear time variant system $\sum(t, \boldsymbol{u}) : \mathbb{R}_0^+ \times \mathbb{R}^m \to \mathbb{R}^p$ with uncertain dynamics with the system input vector $\boldsymbol{u}(t) \in \mathbb{R}^m$ and the measurement vector $\boldsymbol{y}(t) \in \mathbb{R}^p$ and the cost function $J(\boldsymbol{y})$.

Assumption 1. The system is either asymptotically stable or stabilized by an underlying control loop.

Assumption 2. The system dynamics are slower than the dynamics of the perturbation signal of the ESC and therefore also slower than the dynamics of the measurable cost function so that the influence of the system dynamics on the cost function can be neglected.

For the ESC to be applicable the cost function has to directly depend on the system input so that $J(\boldsymbol{y}) = J(\boldsymbol{u})$. The ESC algorithm consists of an UKF as gradient estimator and an optimization scheme. The cost function

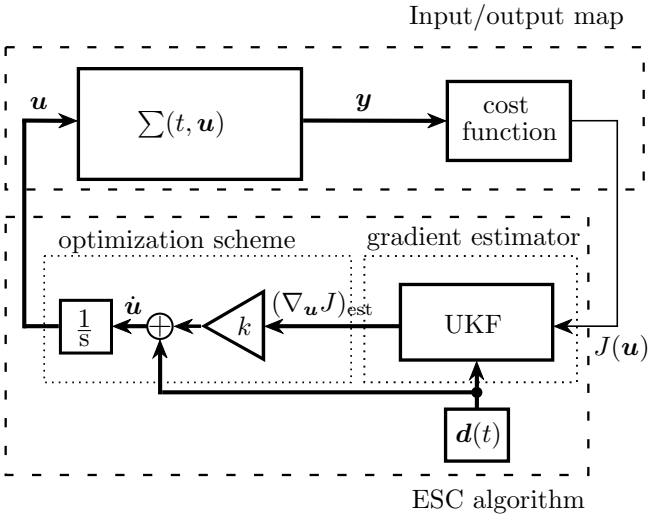

Fig. 1. ESC loop for an asymptotically stable system $\sum(t, \boldsymbol{u})$ with input $\boldsymbol{u}$, output $\boldsymbol{y}$ and cost function $J(\boldsymbol{y}) = J(\boldsymbol{u})$, proposed in Lutz et al. (2019).

serves as input for the UKF which estimates the gradient of the cost function $(\nabla_{\boldsymbol{u}} J)_{\mathrm{est}}$ that is used in the optimization scheme to drive the system $\sum(t, \boldsymbol{u})$ to its maximum or minimum for the control gain $k > 0$ or $k < 0$ in Fig. 1 respectively.

To make the paper self-contained and to motivate the application, the approach proposed in Lutz et al. (2019) is subsequently briefly recalled and summarized. The time derivative of the cost function $J(\boldsymbol{u})$ is given by

$$\frac{\mathrm{d}J(\boldsymbol{u})}{\mathrm{d}t} = \frac{\partial}{\partial \boldsymbol{u}} J(\boldsymbol{u}) \frac{\mathrm{d}\boldsymbol{u}}{\mathrm{d}t}. \tag{1}$$

This can be rewritten in transposed form as

$$\left(\frac{\mathrm{d}\boldsymbol{u}}{\mathrm{d}t}\right)^{\mathrm{T}} \nabla_{\boldsymbol{u}} J(\boldsymbol{u}) = [\dot{u}_1 \cdots \dot{u}_m] \begin{bmatrix} \frac{\partial}{\partial u_1} J(\boldsymbol{u}) \\ \vdots \\ \frac{\partial}{\partial u_m} J(\boldsymbol{u}) \end{bmatrix} \tag{2}$$

with $\nabla_{\boldsymbol{u}} J(\boldsymbol{u})$ denoting the gradient of the cost function with respect to the input vector. The vector of partial derivatives of the cost function with respect to the $n-1$ components of the input vector appended by the cost function is chosen as the UKF estimator states $\boldsymbol{x}(t) \in \mathbb{R}^n$, thus

$$\boldsymbol{x} = \begin{bmatrix} \frac{\partial}{\partial u_1} J(\boldsymbol{u}) \\ \vdots \\ \frac{\partial}{\partial u_m} J(\boldsymbol{u}) \\ J(\boldsymbol{u}) \end{bmatrix} = \begin{bmatrix} x_1 \\ \vdots \\ x_{n-1} \\ x_n \end{bmatrix}, \quad n = m + 1. \tag{3}$$

Since the influence of the system dynamics on the cost function is neglected as mentioned in *Assumption 2* the time derivative of the gradient is modeled as additive white process noise $\hat{\boldsymbol{w}} = [w_1, \ldots, w_{n-1}]^{\mathrm{T}}$ with covariance $Q \in \mathbb{R}_+^{(n-1)\times(n-1)}$. With this the estimator differential equation is given as

$$\dot{\boldsymbol{x}} = \begin{bmatrix} 0 \\ \vdots \\ 0 \\ \dot{\boldsymbol{u}}^{\mathrm{T}} H \boldsymbol{x} \end{bmatrix} + \begin{bmatrix} w_1 \\ \vdots \\ w_{n-1} \\ 0 \end{bmatrix}, \quad t > t_0,\ \boldsymbol{x}(t_0) = \boldsymbol{x}_0 \tag{4}$$

with $H = [I_{n-1}\mathbf{0}_{n-1}] \in \mathbb{R}^{(n-1)\times n}$ where $I_{n-1} \in \mathbb{R}^{(n-1)\times(n-1)}$ is the identity matrix and $\mathbf{0}_{n-1}$ is the zero vector. The time derivative of the system input $\dot{\boldsymbol{u}}(t) \in \mathbb{R}^{(n-1)}$ is obtained by integrating (2)-(4) into the ESC algorithm according to Fig. 1 as

$$\dot{\boldsymbol{u}} = \boldsymbol{d} + k(\nabla_{\boldsymbol{u}} J)_{\text{est}} = \boldsymbol{d} + kH\boldsymbol{x}. \tag{5}$$

Here $\boldsymbol{d}(t) \in \mathbb{R}^{(n-1)}$ is the perturbation signal and k is the scalar gain of the optimization scheme. With $\boldsymbol{w} = [\hat{\boldsymbol{w}}^{\mathrm{T}}\ 0]^{\mathrm{T}}$ the full process model of the gradient estimator reads as

$$\begin{aligned}\dot{\boldsymbol{x}} &= \begin{bmatrix} 0 \\ \vdots \\ 0 \\ \boldsymbol{d}^{\mathrm{T}}H\boldsymbol{x} + k\boldsymbol{x}^{\mathrm{T}}H^{\mathrm{T}}H\boldsymbol{x} \end{bmatrix} + \boldsymbol{w} \\ &= \boldsymbol{f}(\boldsymbol{x}, \boldsymbol{d}) + \boldsymbol{w}, \quad t > t_0, \quad \boldsymbol{x}(t_0) = \boldsymbol{x}_0 \end{aligned} \tag{6a}$$

with the measurement equation

$$y = J(\boldsymbol{u}) + l, \tag{6b}$$

where l denotes white measurement noise with covariance $R > 0$. The output equation of the filter is choosen as

$$\hat{y} = \hat{x}_n + l = h(\hat{\boldsymbol{x}}) + l. \tag{6c}$$

Since a nonlinear filter is needed for the estimation for the nonlinear process model (6) the UKF is used because it is easier to implement and promises more accurate inclusion of the nonlinearities (Julier and Uhlmann, 2004).

Marine boundary layers such as the thermocline are the water layers in which the water properties such as temperature, salinity, density, oxygen, etc. have their maximum gradient with respect to depth. Therefore the cost function is chosen as $\frac{|\Delta P|}{|\Delta z|} = \frac{|P_i - P_j|}{|z_i - z_j|}$, where P is the water property at the location of the AUV, z is the depth of the AUV and $i, j \in \mathbb{N}$ are discrete time indices with $j > i$. The water property and depth measurements are smoothed by a moving average filter to reduce the influence of measurement noise on the ESC loop. To avoid division by zero when the AUV changes its vertical driving direction the cost function is implemented as

$$J(\boldsymbol{y}) = J(\boldsymbol{u}) = \begin{cases} \frac{|\Delta P|}{|\Delta z|} & \text{if } \Delta z > z_{\min} \\ 0 & \text{else} \end{cases}, \tag{7}$$

where $z_{\min}$ is the adjustable minimum depth change. If more than one feature is of interest the cost function can be adapted. A sum of water properties such as temperature, oxygen and salinity measurements could, e.g., be included which would result in searching the mean depth of all involved boundary layers. The system $\sum(t, \boldsymbol{u})$ refers to the AUV within a water body. Hence the system input $\boldsymbol{u}$ defines the desired position of the water property sensor of the AUV, that is assumed to be realized by a suitable controller, and the system output $\boldsymbol{y}$ is the vector of the measured water properties. Since only the depth of the AUV is needed in the cost function the system input is the scalar $u = z$. The position and velocity in x- and y- direction are chosen such that the AUV follows a predefined path.

3. SIMULATION FRAMEWORK

3.1 AUV dynamics

The AUV considered in this paper is the Girona500 AUV from iquarobotics. It is equipped with five thrusters such that the surge, sway, heave, pitch and yaw movements can be controlled. This is an underactuated configuration but the AUV is constructed in such a way that the roll motion is stable. The mathematical model of the AUV considered in this paper reads

$$\dot{\boldsymbol{\eta}} = J_{\boldsymbol{\Theta}}(\boldsymbol{\eta})\boldsymbol{\nu} \tag{8a}$$

$$M\dot{\boldsymbol{\nu}} = -C(\boldsymbol{\nu})\boldsymbol{\nu} - D(\boldsymbol{\nu})\boldsymbol{\nu} + \boldsymbol{\tau}, \tag{8b}$$

where $\boldsymbol{\eta} = [x, y, z, \phi, \theta, \psi]^{\mathrm{T}}$ is the earth fixed position vector (Fossen, 2011). The components x, y, z are defined in the North-East-Down (NED) frame and ϕ, θ, ψ are the roll, pitch and yaw angles. The vector $\boldsymbol{\nu} = [u, v, w, p, q, r]^{\mathrm{T}}$ is the body fixed velocity vector with the entries surge, sway, heave, roll, pitch, and yaw and $\boldsymbol{\tau} = [\tau_u, \tau_v, \tau_w, \tau_p, \tau_q, \tau_r]^{\mathrm{T}}$ is the control vector with the forces τ_u, τ_v, τ_w in surge, sway and heave direction and the roll, pitch and yaw moments τ_p, τ_q, τ_r. Since the Girona500 AUV is underactuated $\tau_p = 0$. Equation (8a) describes the transformation from body fixed into earth fixed coordinates via the rotation matrix $J_{\boldsymbol{\Theta}}(\boldsymbol{\eta})$ while (8b) describes the motion of the ship in body fixed coordinates with the inertia matrix M, coriolis matrix C and damping matrix D. Accurate modeling parameters are not available for the Girona500 AUV so that the mass and damping matrix are implemented as diagonal matrices with estimated parameters based on the specifications by iquarobotics. The underlying motion control system is chosen as a PID controller.

3.2 Simulation environment

The simulations are done in a framework build upon the Robot Operating System (ROS), Gazebo and the unmanned underwater vehicle (UUV) simulator introduced in Manhães et al. (2016). Gazebo is a robot simulator with build in physics engines that yields realistic robot motions. It is build for land based robots, therefore the UUV simulator is used which integrates the hydrodynamic forces and moments in the Gazebo physics engine. ROS can be seen as the middleware for the other two as it provides helper functions such as a library for coordinate transformations and message-passing.

3.3 Simulation data

Environmental data such as conductivity, temperature, depth (CTD) and oxygen measurements is typically only available as a one-dimensional depth profile for distinct latitude and longitude positions. These profiles are sampled with a towed CTD that is operated with a winch installed on a ship. Typically samples are taken several sea miles apart from each other and also data from ocean models with small grid sizes is in a range of one to several sea miles. These large distances are far beyond the coverage of the Girona500 AUV and meaningful interpolation of the data to achieve a resolution of a few meters grid size is not possible. Thus small scale changes in the thermocline

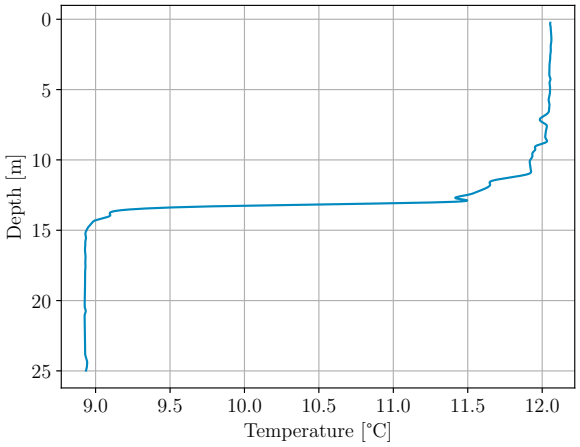

Fig. 2. Temperature profile 1 obtained in the North Sea.

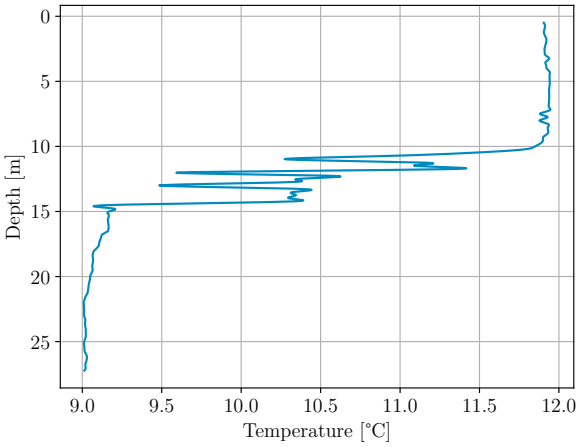

Fig. 3. Temperature profile 2 obtained in the North Sea with zigzag evolution of the thermocline.

have to be artificially simulated by extrapolating the one dimensional profile with respect to x, y and t. This is done in two ways in this paper. First, the original CTD profile $\mathrm{CTD}(z)$ is shifted with respect to x and y by

$$\mathrm{CTD}_{\mathrm{mod}}(x,y,z) = \mathrm{CTD}\left(z + \frac{x}{m_x} + \frac{y}{m_y}\right) + h \tag{9}$$

leading to a sloped plane. Here $\mathrm{CTD}_{\mathrm{mod}}(x,y,z)$ is the artificially modified CTD profile, m_x and m_y are the slopes in x and y direction respectively and h is white measurement noise, implemented as Gaussian noise with standard deviation σ_h. Second, the CTD profile is additionally modulated with a sine wave as

$$\begin{aligned}&\mathrm{CTD}_{\mathrm{mod,\,sin}}(x,y,z,t,\boldsymbol{A}_w,\boldsymbol{f}_w,\boldsymbol{v}_w)\\ &= \mathrm{CTD}\Big(z + \frac{x}{m_x} + \frac{y}{m_y}\\ &\quad + A_{w,x}\sin(2\pi f_{w,x}t + v_{w,x}x)\\ &\quad + A_{w,y}\sin(2\pi f_{w,y}t + v_{w,y}y)\Big) + h\end{aligned} \tag{10}$$

to model internal waves. These are waves that form at boundary layers where vertical mixing of the water is prevented due to density differences. Their wavelengths are much longer compared to normal surface waves. Here t is the time and $\boldsymbol{A}_w = [A_{w,x}, A_{w,y}]^{\mathrm{T}}$, $\boldsymbol{f}_w = [f_{w,x}, f_{w,y}]^{\mathrm{T}}$, $\boldsymbol{v}_w = [v_{w,x}, v_{w,y}]^{\mathrm{T}}$ are the vectors of the amplitude, frequency, and velocity of the internal waves in x and y direction respectively. The CTD profiles that are used in this paper were acquired by the Royal Netherlands Institute for Sea Research (NIOZ) during a cruise on RV Pelagia in June 2012 (64PE354) in the North Sea and are shown in Fig. 2 and 3. Fig. 2 shows a very narrow profile and Fig. 3 shows a profile with a thicker boundary layer that evolves in a zigzag way.

4. SIMULATION RESULTS

Without loss of generality in the following temperature is considered as an example of a water property to make this method comparable with the existing thermocline tracking methods.

All ESC implementations have in common that a gradient of the cost function has to be present for successful operation, consequently the cost function must not be zero in the working point at the start time of the ESC. However this is the case close to the sea surface for a significant number of CTD profiles including the temperature profiles in Fig. 2 and 3. Therefore the algorithm is implemented in a two stage approach. The AUV descends with constant z-velocity in case it is closer to the sea surface than to the sea floor and ascends otherwise. The ESC procedure is started as soon as $J(\boldsymbol{y}) > J_{\mathrm{thr}}$, where J_{thr} is a small parameter compared to the expectable average cost function. For the perturbation signal $d(t)$ a cosine wave is used. The simulation parameters used to produce the presented results are given in Tab. 1.

Table 1. ESC parameters used in simulations.

Period perturbation signal T_{p}	33 s
Amplitude perturbation signal A_{p}	0.02 m
Signal shape perturbation signal	cosine
Optimization gain k	$3 \cdot 10^{-4}$
Covariance Q, R	$3 \cdot 10^{-5}$
Parameter UKF α	1
Parameters UKF β, γ	0
Minimum depth change z_{min}	0.18 m
AUV surge speed u	$0.4\,\frac{\mathrm{m}}{\mathrm{s}}$
Moving average window length t_{win}	3 s
Standard deviation σ_h	0.05

4.1 Thermocline tracking along a straight path

The standard use case for thermocline tracking is the detection and tracking along a straight path because large water bodies are typically rather homogenous in small time and spatial scales. To show that the proposed method is able to detect and track a dynamic boundary layer the CTD profile from Fig. 2 is modulated according to (9). Here $m_x = 50$, $m_y = \infty$ and the AUV is driving in x-direction. The simulated depth of the AUV and corresponding temperature over time are shown in Fig. 4 for a 200 m section. The plot at the top shows the depth of the AUV in solid and the mean thermocline layer in dashed. It can be seen that the UKF based extremum seeking starts before the AUV reaches the mean thermocline. Within a few periods of the perturbation signal the ESC loop reaches the optimal working point and tracks its changes. This is achieved even tough the

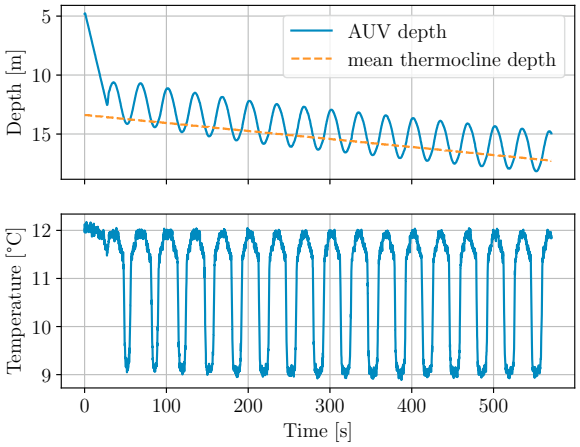

Fig. 4. Depth and temperature measurements for the UKF based ESC for thermocline tracking along a 200 m section in x-direction; the CTD profile from Fig. 2 is modulated according to (9) with $m_x = 50$, $m_y = \infty$.

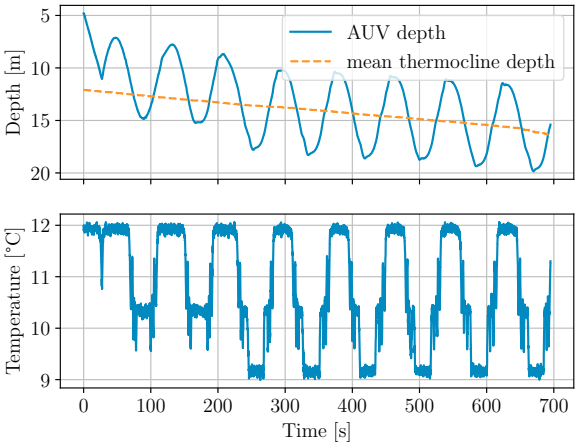

Fig. 5. Depth and temperature measurements for the UKF based ESC for thermocline tracking along a 200 m section in x-direction; the CTD profile from Fig. 3 is modulated according to (9) with $m_x = 50$, $m_y = \infty$.

thermocline has a negative slope in the driving direction of the AUV. Compared to the traditional methods of Cruz and Matos (2010a,b); Zhang et al. (2010); Zhang et al. (2012); Petillo et al. (2010) the presented method reaches the optimal working point later but it does not rely on thresholds in its tracking phase. Due to the regular perturbation signal the AUV samples the thermocline region in a constant fashion. If the amplitude of the ESC is chosen sufficiently large sampling of the whole thermocline is ensured. This is especially advantageous in cases, where the thermocline does not evolve in a smooth way but in a zigzag way. The combination of regular sampling, a sufficiently large perturbation amplitude and the iterative gradient estimation by the UKF makes the method less prone to measurement noise and small scale changes in the boundary layer. In contrast the turning point of the AUV in the traditional methods depends on a threshold of the gradient so that the ascend and descend legs can have different length that are influenced by measurement noise and small scale changes as in the cases, where the thermocline evolves in a zigzag way. In the temperature plot at the bottom of Fig. 4 it can be seen that the whole temperature range from approx. 9 °C to 12 °C is covered already from the beginning of the ESC procedure at $t \approx 30$ s. This is mainly due to the fact that the temperature profile is relatively sharp so that the transition from a gradient near zero to the maximum gradient is fast. Nevertheless it can be seen that the working point at the beginning is sub-optimal because the time in which the AUV measures approx. 9 °C is much shorter than the time in which it measures approx 12 °C. This time difference is reduced as the AUV approaches its optimal working point. In this context the working point refers to the mean depth of the AUV within one perturbation period.

To demonstrate the performance of the proposed method in a more complex environment simulation results are provided in Fig. 5 for CTD profile 2 shown in Fig. 3. As in the previous case the plot at the top shows the depth of the AUV in solid and the mean thermocline layer in dashed and the plot at the bottom shows the temperature over time. Since the boundary layer thickness is larger for this profile than for the previous one also the ESC parameters need to be slightly adjusted to ensure sampling of the whole boundary layer and to stay within the power limits of the thrusters of the AUV. The amplitude and period length of the perturbation signal and the optimization gain k are chosen as $A_\mathrm{p} = 0.04$ m, $T_\mathrm{p} = 83$ s and $k = 7 \cdot 10^{-4}$. All other parameters are chosen as in Tab. 1. Fig. 5 (top) confirms that the UKF based ESC is able to track the challenging temperature profile. Fig. 5 (bottom) shows that different to the previous case the temperature range is not covered right from the beginning but that the last segment of the boundary layer from approx. 9.1 °C to 10.4 °C is missed. The UKF based ESC is able to fine tune the AUV depth within three perturbation signal periods so that the whole boundary layer is sampled. This indicates that the UKF based ESC is able to cope with complex real world scenarios.

4.2 Thermocline tracking within a horizontal grid

Another use case is the tracking of boundary layers within a horizontal grid. Thereby marine features such as small scale eddies and oxygen depleted regions can be detected and mapped in an efficient way but also small scale variations in the boundary layer itself can be measured. In this scenario the AUV was programmed to track the thermocline and simultaneously follow a lawn mover pattern with a size of 130×130 m with a line spacing of 5 m. The CTD profile from Fig. 2 was modulated according to (9) with $m_x = 50$, $m_y = -50$. The simpler temperature profile 1 is used here because the interpretation and visualization of the results is easier in this case. Fig. 6 shows the AUV depth and the mean thermocline depth with respect to time. To keep the plot clearly arranged only the first hour of the AUV mission is shown. By comparing the mean thermocline depth with the average AUV depth it can be observed that the AUV follows the linear thermocline changes with only a small delay. Fig. 7 shows the median depth of the thermocline as an interpolated surface. For this the x, y, z coordinates corresponding to the maximum gradient of the descent and ascend legs are extracted

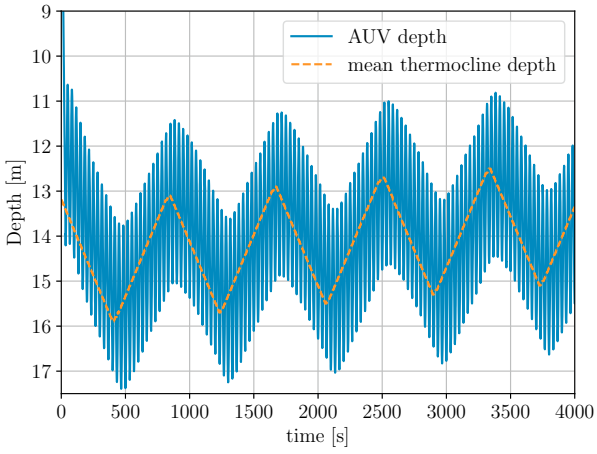

Fig. 6. Depth of the AUV and mean thermocline depth for the first 4000 s for a lawn moving pattern with a size of 130 × 130 m, a line spacing of 5 m and the CTD profile from Fig. 2 modulated by (9) with $m_x = 50$, $m_y = -50$.

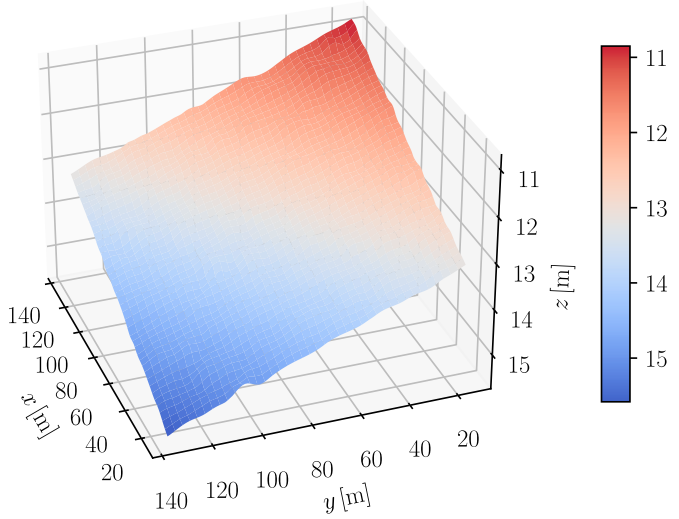

Fig. 7. Interpolated surface plot showing the median depth of the thermocline for a lawn moving pattern with a size of 130 × 130 m, a line spacing of 5 m and the CTD profile from Fig. 2 modulated by (9) with $m_x = 50$, $m_y = -50$.

from the AUV measurements. These distinct points are interpolated which yields the 3D surface in Fig. 7 which is tilted with a positive slope in x- and negative slope in y-direction. This is exactly as expected when the thermocline is modulated according to (9) with $m_x = 50$, $m_y = -50$ so it shows that the UKF based ESC is able to track features that are dynamic in the space domain. In both use cases the feature dynamics are time independent and evolve linearly in space.

Simulation results for a scenario with nonlinear, time dependent dynamics are given in Fig. 8 and 9. Here the AUV was programmed to follow the same path as before but the CTD profile from Fig. 2 was modulated by (10) with $m_x = m_y = \infty$, $\boldsymbol{A}_w = [0, 0.5]^{\mathrm{T}}$, $\boldsymbol{f}_w = [0, \frac{1}{3600\mathrm{s}}]^{\mathrm{T}}$, $\boldsymbol{v}_w = [0, 0.025\frac{\mathrm{m}}{\mathrm{s}}]^{\mathrm{T}}$ to simulate internal waves at the

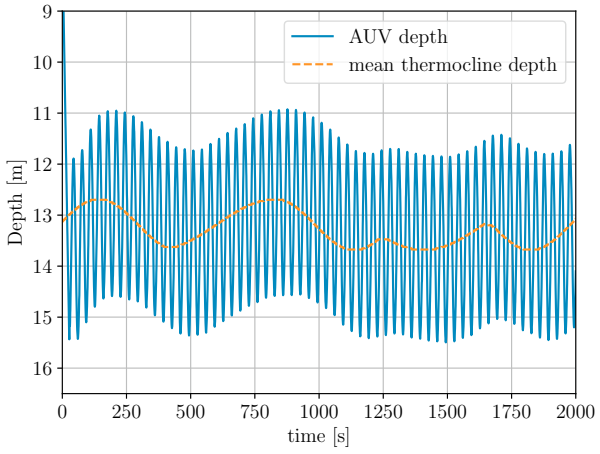

Fig. 8. Depth of the AUV and mean thermocline depth for the first 2000 s of a lawn moving pattern with a size of 130 × 130 m, a line spacing of 5 m with lines parallel to the y axis and the CTD profile from Fig. 2 modulated by (10) with $m_x = m_y = \infty$, $\boldsymbol{A}_w = [0, 0.5]^{\mathrm{T}}$, $\boldsymbol{f}_w = [0, \frac{1}{3600\mathrm{s}}]^{\mathrm{T}}$, $\boldsymbol{v}_w = [0, 0.025\frac{\mathrm{m}}{\mathrm{s}}]^{\mathrm{T}}$ to simulate internal waves.

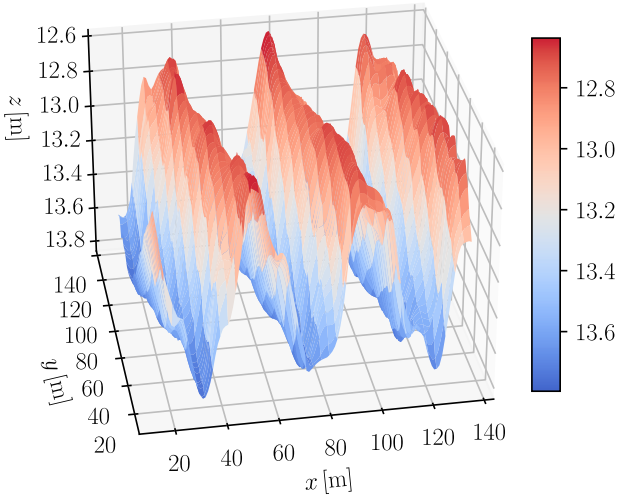

Fig. 9. Interpolated surface plot showing the median depth of the thermocline of a lawn moving pattern with a size of 130 × 130 m, a line spacing of 5 m with lines parallel to the y axis and the CTD profile from Fig. 2 modulated by (10) with $m_x = m_y = \infty$, $\boldsymbol{A}_w = [0, 0.5]^{\mathrm{T}}$, $\boldsymbol{f}_w = [0, \frac{1}{3600\mathrm{s}}]^{\mathrm{T}}$, $\boldsymbol{v}_w = [0, 0.025\frac{\mathrm{m}}{\mathrm{s}}]^{\mathrm{T}}$ to simulate internal waves.

boundary layer. Similar to the previous scenario in Fig. 8 the AUV depth and the mean thermocline depth are plotted with respect to time for the first 30 minutes of the AUV mission. It can be seen that the UKF based ESC is able to track the time varying thermocline with nonlinear dynamics with only a small delay. In Fig. 9 the median depth of the thermocline as an interpolated surface is shown, calculated the same way as for Fig. 7. In this plot the internal wave fronts can be clearly seen but the interpretation of the wave propagation direction is difficult for this time varying feature. This is because of the fact that the interpolated surface can not be treated

as a snapshot of the situation, instead the AUV motions as well as possible feature dynamics have to be considered for a successful interpretation of the results. If the surface would be a snapshot one would intuitively know that the waves propagate mainly in x-direction. But for a time varying thermocline this intuition is wrong. Instead, the AUV track that was designed as lawn mower pattern with the long sections parallel to the y-axis has to be considered as well as all possible wave propagation directions. As a human one can see that the wave has a long wavelength and propagates mainly in negative y-direction. This can be concluded from the fact that the AUV speed $u = 0.4\,\frac{\mathrm{m}}{\mathrm{s}}$ is much faster than the internal wave propagation velocity so that the AUV crosses each internal wave front multiple times and each time the wave propagated a little bit further to the negative y-direction resulting in the seemingly diagonal wave fronts in Fig. 9.

5. CONCLUSION

An UKF based ESC approach is presented for tracking of boundary layers such as the thermocline with an AUV. The proposed approach is a generic method that generates smooth AUV paths and results in a constant sampling of the boundary layer. Parameters corresponding to similar features such as temperature, salinity and oxygen can easily be included in the cost function of the ESC loop. Two essential drawback of ESC are that first a gradient is needed at all times and second that it is challenging to overcome local extrema. The first is addressed by introducing a two stage approach where the AUV is first driven to a region, where a gradient is present and only then the ESC is started. The second can, e.g., be addressed by a suitably large perturbation amplitude in the case of small local extrema and an initial complete dive in case of large local extrema. Here the complete dive has to be analyzed and the ESC has to be started in the vicinity of the global extremum. The efficiency of the proposed method is presented by a set of simulations for scenarios with time independent and time dependent feature dynamics. Future work will include the test of the proposed method with the real AUV as well as research in the field of automated tuning of ESC parameters such as the amplitude and frequency of the perturbation signal. By this the influence of a priori knowledge or estimation of the boundary layer parameters on the tracking performance can be reduced. Further the automated interpretation of the results from AUV missions in areas with time dependent, dynamic features will be investigated.

REFERENCES

Antunes, H. M., Cruz, N. A., 2019. Autonomous identification and tracking of thermoclines with a vertical profiler using extremum seeking control. In: OCEANS 2019 MTS/IEEE SEATTLE. pp. 1–6.

Bhattacharjee, D., Subbarao, K., 2021. Extremum seeking control with attenuated steady-state oscillations. Automatica 125, 109432.

Cruz, N. A., Matos, A. C., 2010a. Adaptive sampling of thermoclines with autonomous underwater vehicles. In: OCEANS 2010 MTS/IEEE SEATTLE. pp. 1–6.

Cruz, N. A., Matos, A. C., 2010b. Reactive auv motion for thermocline tracking. In: OCEANS'10 IEEE SYDNEY. pp. 1–6.

Fossen, T. I., 2011. Handbook of Marine Craft Hydrodynamics and Motion Control.

Julier, S., Uhlmann, J., 2004. Unscented filtering and nonlinear estimation. Proceedings of the IEEE 92 (3), 401–422.

Krstić, M., Wang, H. H., 2000. Stability of extremum seeking feedback for general nonlinear dynamic systems. Automatica 36 (4), 595–601.

Lutz, M., Freudenthaler, G., Roduner, C., Meurer, T., 2019. Ukf-based constrained extremum-seeking control with application to a large-bore gas engine. In: 2019 IEEE 58th Conference on Decision and Control (CDC). pp. 561–566.

Manhães, M. M. M., Scherer, S. A., Voss, M., Douat, L. R., Rauschenbach, T., sep 2016. UUV simulator: A gazebo-based package for underwater intervention and multi-robot simulation. In: OCEANS 2016 MTS/IEEE Monterey. IEEE.

MarketsandMarkets, 2020. marketsandmarkets. URL `https://www.marketsandmarkets.com/Market-Reports/autonomous-underwater-vehicles-market-141855626.html`

Petillo, S., Balasuriya, A., Schmidt, H., 2010. Autonomous adaptive environmental assessment and feature tracking via autonomous underwater vehicles. In: OCEANS'10 IEEE SYDNEY. pp. 1–9.

Radut, M., 2017. Analysis of the advanced esc algorithm to accurately find the extremes on multimodal benchmark patterns. In: 2017 9th International Conference on Electronics, Computers and Artificial Intelligence (ECAI). pp. 1–6.

Scheinker, A., Scheinker, D., 2016. Bounded extremum seeking with discontinuous dithers. Automatica 69, 250–257.

Zhang, Y., Bellingham, J. G., Godin, M., Ryan, J. P., McEwen, R. S., Kieft, B., Hobson, B., Hoover, T., 2010. Thermocline tracking based on peak-gradient detection by an autonomous underwater vehicle. In: OCEANS 2010 MTS/IEEE SEATTLE. pp. 1–4.

Zhang, Y., Bellingham, J. G., Godin, M. A., Ryan, J. P., 2012. Using an autonomous underwater vehicle to track the thermocline based on peak-gradient detection. IEEE Journal of Oceanic Engineering 37 (3), 544–553.